

# Temporally Consistent Dynamic Scene Graphs: An End-to-End Approach for Action Tracklet Generation

Raphael Ruschel  
UC Santa Barbara  
raphael1251@ucsb.edu

Md Awsafur Rahman  
UC Santa Barbara  
awsaf@ucsb.edu

Hardik Prajapati  
UC Santa Barbara  
hprajapati@ucsb.edu

Suya You  
ARL West  
suya.you.civ@army.mil

B. S. Manjunath  
UC Santa Barbara  
manj@ucsb.edu

## Abstract

*Understanding video content is pivotal for advancing real-world applications like activity recognition, autonomous systems, and human-computer interaction. While scene graphs are adept at capturing spatial relationships between objects in individual frames, extending these representations to capture dynamic interactions across video sequences remains a significant challenge. To address this, we present TCDSG – Temporally Consistent Dynamic Scene Graphs – an innovative end-to-end framework that detects, tracks, and links subject-object relationships across time, generating action tracklets—temporally consistent sequences of entities and their interactions. Our approach leverages a novel bipartite matching mechanism, enhanced by adaptive decoder queries and feedback loops, ensuring temporal coherence and robust tracking over extended sequences. This method not only establishes a new benchmark by achieving over 60% improvement in temporal recall@k on the Action Genome, OpenPVSG, and MEVA datasets but also pioneers the augmentation of MEVA with persistent object ID annotations for comprehensive tracklet generation. By seamlessly integrating spatial and temporal dynamics, our work sets a new standard in multi-frame video analysis, opening new avenues for high-impact applications in surveillance, autonomous navigation, and beyond.*

## 1. Introduction

Understanding and detecting actions in videos is a critical task for numerous applications, including monitoring [30], human-computer interaction [5, 36], and autonomous systems [1]. Traditionally, static scene graphs are used to capture relationships between objects within individual frames. However, these methods frequently fall short in preserving

object relationships over time, which is crucial for consistently tracking interactions throughout an entire video sequence. Figure 1 presents an example of an input video sequence and the corresponding desired output that includes a triplet  $\langle \text{subject}, \text{object}, \text{relationship} \rangle$ , along with bounding boxes and timestamps to denote the activity.

Recent advances in action detection and scene graph generation have enabled models to capture spatial relationships within individual frames [16, 17, 48]. While some methods tackle challenges like compositionality [18] and long-tailed dataset biases [35], few explore the need for temporal coherence across frames. Existing frame-by-frame approaches often rely on post-processing to aggregate results over time [25, 56]. This approach inherently limits the use of temporal cues, hindering the creation of action tracklets that are consistent across the video. Thus, a major challenge is to preserve object associations and relationships over time without extensive post-processing.

To tackle this challenge, we introduce TCDSG—Temporally Consistent Dynamic Scene Graphs—an innovative end-to-end pipeline designed to generate seamless action tracklets across entire video sequences. By integrating our approach into existing architectures with minimal modifications, we achieve substantial gains in temporal consistency for both object tracking and relationship prediction, pushing the boundaries of video understanding.

We evaluate TCDSG on three benchmark datasets—Action Genome, OpenPVSG, and MEVA—demonstrating state-of-the-art performance in tracklet consistency and competitive framewise prediction. Additionally, we provide a new set of annotations for a subset of the MEVA dataset, where we uniquely identify each object, further validating our approach.

Our main contributions are as follows:

- **A Novel Bipartite Matching Mechanism for Tempo-**

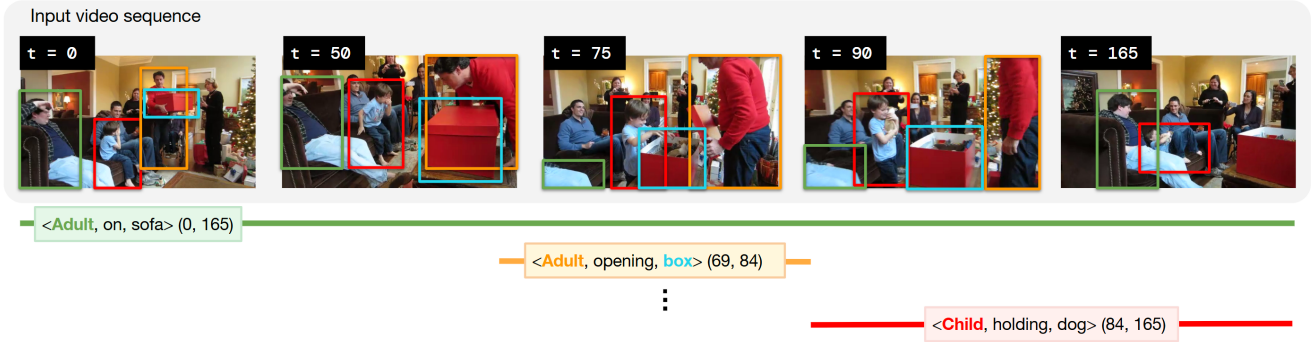


Figure 1. An example of the desired output for a video sequence. At the top, we show a few selected frames and their corresponding timestamp, and at the bottom, distinct action tracklets. Each interaction displays a triplet  $\langle$ subject, object, relationship $\rangle$  alongside the associated bounding box (color-coded) and timestamps. For clarity, only select interactions are annotated.

**ral Consistency:** We introduce a new approach to bipartite matching that prioritizes temporal coherence across frames, addressing limitations in existing methods and achieving a stable representation of dynamic scenes.

- **End-to-End Scene Graph Generation Framework:** Our approach enables the direct generation of temporally consistent scene graphs from input sequences, eliminating the need for post-processing and enhancing accuracy in evolving scene relationships.
- **Enhanced MEVA Dataset Annotations:** We provide unique, persistent object IDs in a subset of the MEVA dataset, enabling more advanced tracklet generation and establishing a foundation for further research in dynamic scene understanding.

## 2. Related works

### 2.1. Scene Graph Generation

Scene graph generation (SGG) involves creating a graph-like structure where nodes represent objects in a scene and edges represent relationships between these objects, such as actions (e.g., *holding*, *sitting*, *walking*) and spatial relationships (e.g., *close*, *to the right of*, *above*). Originally introduced for image retrieval [22], SGG has since become foundational for applications in monitoring, interactive systems, and human-computer interfaces. Early work focused on *static SGG*, generating scene graphs for single images [4, 7, 8, 33, 40, 43, 45, 51, 52].

Considerable effort has been devoted to tackling challenges in SGG, such as compositionality and dataset biases. For instance, [18] examines compositional SGG to improve recall for unseen triplets formed from known objects and relationships, and also discusses limitations of the two-stage SGG pipeline used in [13, 27, 31, 45, 46, 50]. Additionally, addressing biases from long-tailed distributions is an ongoing focus [32, 35], with recent methods employing causal

inference [32] and Gaussian Mixture Models [35] to create balanced predictions.

Recent advancements have expanded SGG to dynamic scenes [9, 21, 29, 44, 58], aiming to generate scene graphs across video sequences by harnessing temporal context. Unlike static SGG, dynamic SGG captures time-dependent actions (e.g., *picking up* vs. *putting down*), which require an understanding of temporal dependencies. Temporal consistency becomes essential here, as it supports the accurate interpretation of activities that evolve over time.

An important development in this field is Panoptic Video Scene-Graph Generation (PVSG) [56], which introduces action tracklets for temporal activity understanding. This work also proposes the use of panoptic segmentation masks instead of bounding boxes, achieving pixel-level localization for subjects and objects. However, this approach depends on post-processing to aggregate results over time, limiting its utility for applications that require temporal consistency in an end-to-end framework.

### 2.2. Tracking

Object tracking in computer vision focuses on detecting and following objects throughout video sequences to capture their trajectories, a capability essential for applications like autonomous driving, surveillance, action recognition, and augmented reality. Traditional approaches, including Kalman filters [54] and mean-shift algorithms [59], have evolved with deep learning to form sophisticated multi-object tracking (MOT) systems based on CNNs and transformers.

Many approaches [2, 24, 38, 55] address tracking as a combination of appearance and motion cues. Here, appearance features are matched using re-identification (Re-ID) metrics, while motion is modeled using techniques like Kalman filtering [54] and Intersection over Union (IoU) for location prediction. However, post-processing to merge ap-

pearance and motion often results in suboptimal temporal dependency modeling across frames, limiting its effectiveness for tracking continuous actions. TransTrack [42], for example, uses a transformer-based approach for bounding box generation but requires post-processing for IoU-based matching.

More recently, end-to-end tracking architectures have emerged, where detection and association are learned within a unified framework. MOTR [57] and TrackFormer [34] extend DETR [3] by treating tracking as a *tracking-by-attention* task, using attention maps for both tracking and detection. MOTR’s tracklet-aware label assignment scheme manages new and stale tracklets dynamically through variable-length track queries.

Despite significant progress, existing methods fall short of unifying activity recognition and object tracking within a fully end-to-end framework. Current approaches tend to treat these tasks in isolation, missing the opportunity to leverage their synergy. This gap highlights the need for integrated solutions capable of simultaneously capturing complex interactions and object trajectories, which is crucial for advancing applications like trajectory analysis, seamless human-computer interaction, and real-time monitoring in dynamic environments.

### 3. Methodology

#### 3.1. Problem Formulation

Given an input video sequence  $\mathbf{V} = \{\mathbf{I}_1, \mathbf{I}_2, \dots, \mathbf{I}_T\}$  with  $T$  frames, the task is to generate a set of action tracklets  $\mathbf{AT} = \{\mathbf{at}_1, \mathbf{at}_2, \dots, \mathbf{at}_M\}$ , where  $M$  is the number of distinct activities in video  $\mathbf{V}$ . Each tracklet  $\mathbf{at}_i \in \mathbf{AT}$  is represented by  $\langle s_i, o_i, r_{so}, \mathbf{SB}, \mathbf{OB}, t_{start}, t_{end} \rangle$ , where:

- $s_i$  and  $o_i$  denote the subject and object class labels,
- $r_{so}$  indicates the relationship between the subject and object,
- $t_{start}$  and  $t_{end}$  are the starting and ending frames of the action tracklet,
- $\mathbf{SB}$  and  $\mathbf{OB}$  are sets of bounding boxes that capture the spatial locations of the subject and object from  $t_{start}$  to  $t_{end}$ , respectively.

These bounding boxes provide spatial continuity, ensuring precise localization of subjects and objects throughout each activity.

#### 3.2. Network Architecture

Our network architecture draws inspiration from the decoupled design of transformer-based systems, where backbone features are shared across two independent branches, such as the ones in DDS [18]. The first branch (object branch) is dedicated to generating subject/object labels and their bounding boxes, while the second branch (relation branch) focuses on predicting predicates that define object interac-

tions. This innovative approach, which achieves state-of-the-art results on a selected benchmark dataset, establishes a strong baseline for further enhancement. However, unlike existing architectures that primarily focus on single-class subjects (e.g., *Person* in Action Genome), we expand the scope by introducing a third, specialized ‘subject branch’ to handle multiple subject classes, thereby significantly increasing the model’s versatility (Figure 2).

The base architecture is derived from DETR [3], which has demonstrated success in object detection. However, Deformable DETR [60] offers improved multi-scale detection and faster convergence, making it more suited for dynamic scenes with objects of varying sizes and movements. By incorporating deformable attention mechanisms, we align our model with Deformable DETR to handle such diversity. This allows the model to adaptively adjust to different scales and movements without relying on static reference points, which can limit performance in rapidly changing scenes.

Our approach introduces a dynamic query mechanism that adapts query embeddings to each input frame. Instead of using static queries as in DETR, we generate initial reference points by applying cross-attention between encoder feature vectors and learnable queries. Furthermore, we insert embeddings from the previous frame into the current frame, ensuring temporal smoothness and capturing frame-to-frame correlations. This adaptive mechanism enhances temporal consistency in predictions by adjusting to dynamic scene changes, improving the stability of the generated tracklets (see Figure 3 for a detailed illustration).

#### 3.3. Temporal Hungarian Matching

DETR-based architectures conceptualize object detection as a set prediction problem, where the network generates a set of predictions based on a specified number of queries ( $N_q$ ). To align these predictions with ground-truth labels during training, the Hungarian algorithm is typically employed. Previous HOI models [9, 18, 49] generally treat each frame as an isolated instance, overlooking temporal coherence. In contrast, our approach introduces a novel mechanism to ensure consistency across frames, enabling more accurate and continuous tracking of interactions over entire video sequences.

After a ground-truth object is linked to a specific query, subsequent frames enforce that association, ensuring that the same triplet is consistently maintained throughout the video sequence. This process is managed via a hashmap that records each unique triplet—composed of  $\langle$ subject ID, object ID, and relationship $\rangle$  identifiers—and maps it to its initially assigned query. In later frames, previously observed triplets are automatically matched with their assigned queries. A high cost (e.g.,  $10^6$ ) is then added to the corresponding row of the cost matrix, reinforcing the initial assignment and preventing other triplets from being linked

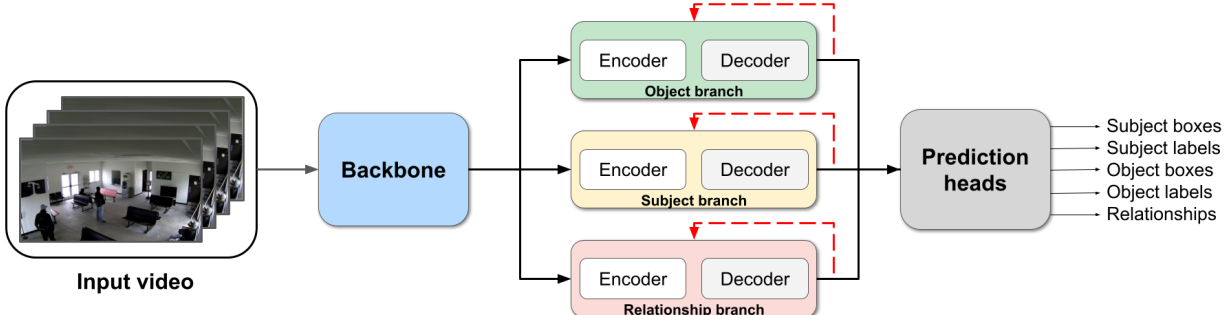


Figure 2. Network architecture of our proposed method. A CNN backbone extracts features, which are shared across three branches, enabling the model to independently predict subject, object, and relationship labels. Red arrows indicate feedback loops, which takes the output of the decoder from frame  $t - 1$  and mix them with the input queries of frame  $t$  using a cross-attention operation. This aids the decoding and reference point generation by conditioning the process based on the information seen previously.

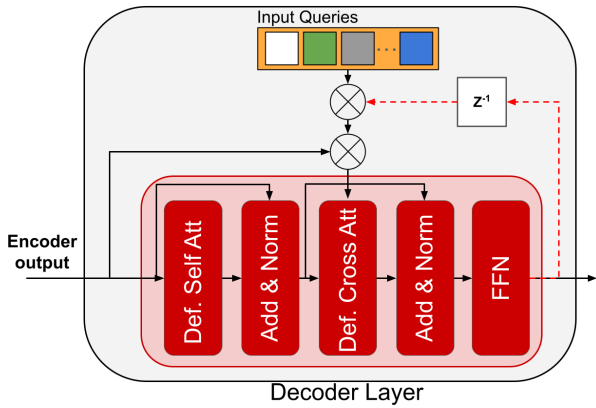


Figure 3. Detailed architecture of the decoder used in all 3 branches of our network. Note the connection between the output of the encoder, the feedback from the output of the decoder, and the input queries. This scheme is used to feed information from both the previous frames and from the current one to the decoding process, improving the generation of the initial reference points.  $\otimes$  indicates the standard cross-attention operation.

to that query.

For bipartite matching between the predictions  $\mathbf{P}_t$  of frame  $\mathbf{I}_t$  and the corresponding ground truth  $\mathbf{G}_t$ , we utilize the same cost functions as in [3]:  $\mathbf{C}_o^{i,j}$ ,  $\mathbf{C}_r^{i,j}$ , and  $\mathbf{C}_s^{i,j}$ , representing the matching costs for the object, relationship, and subject classes (where applicable). Additionally,  $\mathbf{C}_{ob}^{i,j}$ ,  $\mathbf{C}_{ub}^{i,j}$ , and  $\mathbf{C}_{sub}^{i,j}$  represent the costs associated with object, union, and subject bounding boxes, respectively. Here,  $i$  denotes the  $i^{th}$  entry in the prediction set  $\mathbf{P}_t$ , while  $j$  denotes the  $j^{th}$  entry in the ground-truth set  $\mathbf{G}_t$ . Notably, the union box used in  $\mathbf{C}_{ub}^{i,j}$  is the union of the subject and object boxes, and is used during training to guide the relationship branch by refining spatial alignment for relationship prediction.

### 3.4. Loss Functions

After performing the Hungarian matching between predictions and ground-truth, we utilize standard loss functions commonly employed in the literature [3, 60]. Our final loss function is defined as follows in Eq. (1).

$$\mathcal{L} = \lambda_g \mathcal{L}_{GIOU} + \lambda_l \mathcal{L}_{L1} + \lambda_o \mathcal{L}_{obj} + \lambda_r \mathcal{L}_{rel} \quad (1)$$

where  $\mathcal{L}_{GIOU}$  and  $\mathcal{L}_{L1}$  are the generalized intersection over union (gIOU) and L1 box regression losses, applied to the predicted bounding boxes for subjects, objects, and relation regions.  $\mathcal{L}_{obj}$  is the cross-entropy loss for subject and object label predictions, while  $\mathcal{L}_{rel}$  represents the focal loss for the relationship label predictions. The hyperparameters  $\lambda_g$ ,  $\lambda_l$ ,  $\lambda_o$ , and  $\lambda_r$  are used to balance the contributions of each loss term, allowing us to adjust the emphasis on spatial accuracy versus label accuracy.

To further refine feature representations, we incorporate a cosine similarity-based contrastive loss term. This loss encourages feature representations for the same class to remain consistent across frames while maximizing separation between different classes. To compute this term, we maintain a running average of the decoder features for each object and relationship class. The contrastive loss is formulated as shown in Eq. (2).

$$\mathcal{L}_{CS} = \text{CS}(\mathbf{v}_{\text{feat}}^i, \mu_{\text{feat}}^i) - \text{CS}(\mathbf{v}_{\text{feat}}^i, \mathbf{v}_{\text{feat}}^{\neg i}), \quad (2)$$

where  $\mathbf{v}_{\text{feat}}^i$  is the feature vector for class  $i$ ,  $\mu_{\text{feat}}^i$  represents a running average of features for class  $i$ , and  $\mathbf{v}_{\text{feat}}^{\neg i}$  includes features of other classes. This contrastive mechanism strengthens temporal stability by maintaining consistent intra-class feature representations across frames, which is critical for generating coherent tracklets in dynamic scenes.

Together, these loss components support spatial accuracy, semantic fidelity, and temporal stability, enabling robust, temporally consistent action tracklet generation.

### 3.5. Evaluation Metrics

To align with the literature, we adopt the temporal Recall@K (tR@K) metric used by [56], extending the base Recall@K metric to capture the temporal aspect of action tracklets. Unlike traditional Recall@K, which treats each frame independently, tR@K evaluates whether predicted tracklets maintain temporal consistency across the sequence. For a prediction to be correct under the standard Recall@K metric, the predicted triplet  $\langle s, o, r_{so} \rangle$  must match the ground truth, and the bounding boxes for subject and object must have an IoU above a threshold, commonly set to 0.5.

To incorporate temporal information, we consider a prediction tracklet correct if it also achieves a temporal IoU above a specified threshold, meaning the predicted time range  $\langle t_{start}, t_{end} \rangle$  must have a minimum overlap with the ground-truth timestamp. If a prediction passes this temporal IoU threshold, Recall@K is calculated based on the frames that overlap in time, effectively assessing whether the model captures continuous and accurate subject-object relationships throughout an activity. If a tracklet passes the temporal IoU threshold, contains the correct triplet, and an average bounding box IoU above 0.5 for the overlapping timestamp, then the tracklet is marked as correct.

For a more detailed evaluation, we also report mean Recall@K (mR@K), which computes recall for each predicate individually before averaging across classes. This metric is particularly useful for datasets with long-tailed distributions as each class will have the same weight during the averaging operation.

We report our performance using only the SGDet protocol [20], as it aligns with our model’s end-to-end design. SGDet requires predicting the complete triplet—subject, object, relationship, and bounding boxes—in a single step, making it a natural fit for our one-stage scene graph generation. Alternative protocols like PREDCLS and SGPRED are less compatible with one-stage methods, as they typically decouple relationship and object predictions, which would conflict with our integrated approach.

Additionally, our model’s design enforces a “With constraint” setting, in which each query predicts only one triplet per frame. This setup prevents redundancy in tracklet generation, enhancing clarity and stability in action tracking. In contrast, a “No constraint” setting would allow multiple predictions per pair based on confidence scores, which would be incompatible with our method and could result in unnecessary overlap in tracklets.

## 4. Datasets

To train and evaluate our method, we selected three datasets that meet the requirements for action tracklet generation, each providing annotations for subject and object classes, their bounding boxes, and the relationships between them. Additionally, since tracking requires consistent identifiers for each subject and object to handle cases with multiple instances of the same class, we adapted each dataset to ensure compatibility with our method. Below, we provide detailed descriptions of each dataset and any modifications applied.

### 4.1. Action Genome

Action Genome (AG) [20], proposed in 2020, is based on the Charades [41] dataset. AG builds on this dataset by adding frame-level scene graph annotations that include subject and object locations, object classes, and relationships. AG consists of 36 distinct object classes and 25 relationship classes across three categories: **Attention** (e.g., *looking, not looking*), **Spatial** (e.g., *close, to the left*), and **Contacting** (e.g., *holding, sitting*). In total, AG provides 1,715,568 instances within 135,484 subject-object pairs, with each pair potentially linked by multiple relationships. However, the subject is always labeled as “person,” and no unique identifiers are provided for tracking purposes.

To enable tracking on AG, we implemented a pseudo-labeling strategy to assign consistent object identifiers. Since AG lacks multiple instances of the same object class per frame, we used bounding box overlap across consecutive frames to assign identifiers. If an object’s bounding box in the current frame overlapped sufficiently with one in the previous frame, we assigned the same identifier. While this may introduce noisy labels if one object exits and another of the same class enters, manual checks indicated that such cases usually involved the same object returning, supporting our approach’s validity.

### 4.2. OpenPVSG

The OpenPVSG dataset was created for the Panoptic Video Scene Graph Generation (PVSG) [56] task, which expands the traditional scene graph generation task to include pixel-level segmentation masks instead of bounding boxes. This dataset consists of 400 videos averaging 76.5 seconds in length (5 FPS) and was assembled from VidOR [39], EpicKitchen [11], and Ego4D [14], resulting in a diverse collection of indoor and outdoor scenes with both moving and fixed cameras. Unlike AG, OpenPVSG includes various subjects beyond “person” and provides unique identifiers for each object in a video sequence, making it inherently suitable for tracking tasks.

OpenPVSG contains 157 object classes, including animals, furniture, and food items, and 57 relationship classes. To adapt OpenPVSG to our methodology, we converted

segmentation masks to bounding boxes by taking the minimum and maximum coordinates of each mask as bounding box corners. While our method could be modified to generate segmentation masks instead of bounding boxes, pixel-level localization is not necessary for the vast majority of use cases. Bounding boxes are generally sufficient for object tracking and offer a more computationally efficient solution within our framework.

### 4.3. MEVA

The large-scale MEVA dataset [10] is designed for activity detection in multi-camera environments. It was created under the Intelligence Advanced Research Projects Activity (IARPA) Deep Intermodal Video Analytics (DIVA) program to support DIVA performers and the broader research community. This dataset contains over 9300 hours of untrimmed, continuous video footage spanning a variety of scenarios. MEVA provides annotations for 144 hours of footage across 37 activity types, with corresponding bounding boxes for each instance. Data was collected from approximately 100 actors performing scripted scenarios over three weeks at an access-controlled venue with overlapping and non-overlapping indoor and outdoor scenarios, captured by 38 cameras positioned to mimic typical surveillance setups.

Despite its extensive scope and potential for tracking individuals across multiple cameras, MEVA presents several annotation challenges:

1. Some relationships do not follow the standard  $\langle \text{subject}, \text{object}, \text{relationship} \rangle$  format found in the literature. For instance, annotations such as *vehicle reverses* lack an explicit object.
2. Certain relationship classes incorporate the object within the label (e.g., *person opens facility door* or *person opens vehicle door*), but the corresponding object may lack a bounding box.
3. Annotations were generated using a tracking-based approach where each subject was assigned a track ID intended as a unique identifier. However, this approach often results in multiple identifiers for the same individual within a single video sequence, reducing tracking reliability.

To adapt MEVA for our method, we implemented the following strategies:

1. For activities without an associated object, we exclude object-related losses during training. During inference, we discard object-related predictions if the model predicts these relationships.
2. For cases where relationship classes lack bounding boxes, we manually annotated a subset of instances. For cases we could not annotate, we applied the strategy from (1).

3. We developed an annotation tool to manually correct selected videos, ensuring each subject and object has a unique identifier within each video sequence. Currently, we are working on cross-camera identifier matching to enable tracking across the entire venue.

Using this tool, we assigned unique identifiers to objects in scenes within high-activity areas of interest. Given the dataset's scale and the significant labor required, we focused these corrections on high-traffic regions, where complex interactions are more frequent. MEVA's predominant scenes involve parking lots and roads with simpler activities (e.g., vehicles and people passing by), so concentrating on active regions provides a more efficient use of resources.

After this annotation process, we finalized 141 training videos comprising  $\approx 400k$  frames across 16 cameras. Our test set includes 47 videos over 12 cameras, 3 of them being unseen during training, with  $\approx 23k$  frames.

### 4.4. Implementation Details

We utilize ResNet-50 [15] as the backbone for our model, balancing computational efficiency and detection accuracy, which is crucial for large-scale video data. Training is conducted using the AdamW [19] optimizer, alongside the BLoad [37] strategy to facilitate distributed training across videos of varying lengths. BLoad dynamically balances batch loading across GPUs, preventing deadlocks from gradient synchronization by ensuring uniform batch lengths despite varying video durations.

Each branch of our model uses 6 encoder-decoder layers, with  $N_q = 100$  queries of dimension 256. These choices balance complexity and performance for efficient multi-object tracking across frames. We initialize training from a DETR checkpoint pre-trained on COCO [28], leveraging its strong generalization in object detection tasks. Our model contains 59M parameters and is trained on 8 NVIDIA A100 GPUs, with epoch times ranging from 1 to 4 hours depending on the dataset. The learning rate begins at  $10^{-4}$  and decays by a factor of 0.9 per epoch. Each experiment is run for 20 epochs, with the best checkpoint selected based on evaluation metrics.

We employ basic frame-level augmentations, including color jitter, Gaussian noise, random crops, and resizes. Input frames are resized so that the shortest side is between 480 and 800 pixels, with a maximum length of 800 pixels for the longest side.

During inference, our network generates  $N_q$  predictions, with each prediction assigned a confidence score by multiplying the softmax-transformed logits for object, subject, and relationship components. Predictions are ranked by score, with the top  $k$  selected to construct tracklets by grouping predictions with the same query index. This method enforces temporal coherence in the tracklet, as each query index consistently maps to a unique tracklet. If a

Method	SGDet - With constraint					
	mR@20	mR@50	R@20	R@50	tR@20	tR@50
iSGG [23]	19.7	22.9	29.2	35.3	-	-
STTran-TPI [49]	20.2	21.8	29.1	34.6	-	-
APT [26]	-	-	29.1	38.3	-	-
TEMPURA [35]	22.6	23.7	33.4	34.9	-	-
VsCGG [32]	-	24.2	35.8	38.2	-	-
TD2-Net (p) [29]	-	23	28.7	37.1	-	-
EOD [47]	-	-	40.9	<b>48.9</b>	-	-
DDS [18]	<b>29.1</b>	32.2	<b>42.0</b>	47.3	13.5	18.6
<b>TCDSG (Ours)</b>	26.9	<b>36.4</b>	38	47.8	<b>15.5</b>	<b>30.2</b>

Table 1. Comparison of Recall@k with  $k = \{20, 50\}$  in AG’s test set. We note that while our method suffers a performance degradation for single-frame prediction which we associate to not performing the optimal assignments between predictions and ground-truths during the matching stage. Despite that, our method presents a clear improvement when the temporal aspects of the activities are also considered, yielding 62% improvement on certain scenarios.

query index is absent from the top  $k$  predictions in subsequent frames or predicts a different triplet, a new tracklet for that query index is initialized.

## 5. Results

### 5.1. Performance evaluation

We start by comparing our method to existing state-of-the-art approaches on the Action Genome dataset. Results are presented in Table 1. We take all metrics from other approaches directly from the respective manuscript. Some implementations did not consider some of the metrics we are reporting; these missing entries are denoted as ‘-’ in the results table.

As shown in Table 4, our method achieves competitive performance on single-frame classification tasks, comparable to existing state-of-the-art methods. However, it significantly outperforms others in the tracking task, where prediction consistency across frames is critical. This consistency is essential for applications requiring reliable, long-term tracking of interactions.

Our model’s architecture, with its focus on temporally consistent tracklet generation, is particularly advantageous for multi-frame tracking. By enforcing coherent object and relationship tracking over time, it reduces fragmentation in predictions—a common limitation in frame-by-frame approaches—and yields substantial improvements in temporal Recall@K metrics over single-frame baselines.

For OpenPVSG, we report our results using bounding boxes for spatial localization in Table 2. Additionally, in the supplementary materials, we provide further experiments where segmentation masks are generated from our predictions, followed by a recalculation of the relevant metrics.

Similar to AG, we note a significant improvement in the

Method	R@20	R@50	tR@20	tR@50
IPS + T [6, 53]	-	-	3.88	5.66
VPS [6, 25]	-	-	0.42	0.73
<b>TCDSG*</b>	<b>12.6</b>	<b>20.1</b>	<b>6.0</b>	<b>11.2</b>

Table 2. Results on OpenPVSG dataset. For IPS+T and VPS results, we extracted the numbers from [56]. On our results, \* denotes using bounding boxes as object location grounding.

temporal recall@K over previous methods, highlighting the advantages of our method.

On the MEVA dataset, participants in the DIVA program, such as [12], evaluated their methods using different metrics, primarily Pmiss@Xtfa. Here, Pmiss represents the ratio of activities where the system did not detect the activity for at least one second, while TFA (time-based false alarm rate) measures the portion of time that the system incorrectly detected an activity. Due to differences in evaluation metrics and the fact that we use only a subset of MEVA data with additional annotations from our tool, direct comparisons with DIVA participants are not feasible.

Given that MEVA includes videos up to five minutes long, we leverage this unique property to test our method’s robustness across various video lengths by introducing different subsampling factors for the test data. This approach allows us to assess temporal consistency in conditions ranging from densely sampled sequences to more sparsely sampled ones. Results are shown in Table 3.

As seen in Table 3, temporal Recall@K (tR@K) generally increases with higher subsampling factors. However, this trend highlights a key limitation: stacking predictions solely based on query index can lead to prediction fragmentation due to noise. For example, if a query predicts a triplet

Subsample Factor	R@20	R@50	tR@20	tR@50
1	62.1	67.9	6.7	7.8
5	62.1	67.9	9.9	12.4
10	62	67.7	10.9	17
20	61.9	67.6	17.6	31.2

Table 3. Results on MEVA dataset with different subsampling factors on our proposed test set

$T_1$  consistently over several frames but briefly switches to  $T_2$  before returning to  $T_1$ , this results in three separate tracklets, disrupting continuity. This issue is particularly evident at lower subsampling factors (1 and 5) on longer videos, where actions may span thousands of frames and encounter higher noise levels.

Another limitation is track switching in densely populated scenes, where multiple subjects perform similar activities. In such cases, a query index may briefly switch the tracked subject, leading to failed spatial IoU checks and inaccurate tracking. Addressing these limitations could involve adding identity verification mechanisms or context-aware adjustments to enhance tracklet stability and reduce fragmentation in challenging, high-density environments like those in MEVA.

## 6. Ablation Studies

In this section, we conduct ablation studies to evaluate the impact of each component of our proposed approach. Unless otherwise noted, all experiments were conducted on the Action Genome dataset, which provides a balanced combination of class diversity and data availability.

Table 4 shows the performance of our baseline model and the effect of adding each component on both single-frame predictions (R@k) and activity tracking (tR@k).

Method	R@20	R@50	tR@20	tR@50
(1) Baseline	36.7	44.4	10.2	16.0
(2) Temp. Hung. Matching	34.3	42.0	13.1	25.4
(3) Dynamic queries	39.8	<b>46.9</b>	11.0	16.2
(4) Cos similarity + (2) + (3)	38	<b>47.8</b>	<b>15.5</b>	<b>30.2</b>

Table 4. Performance comparison of our baseline model and the effect of each proposed component on single-frame recall (R@k) and tracking recall (tR@k) at different  $k$  values on the Action Genome dataset.

Our results in Table 4 underscore the transformative impact of each component in our model. By incorporating dynamic queries we significantly boost single-frame recall, as the decoder adapts reference points dynamically to each frame, rather than relying on static initial positions. This

adaptive mechanism optimizes object localization by leveraging frame-specific features, thereby enhancing precision in object detection. Although dynamic queries primarily focus on improving single-frame predictions, their impact on temporal recall remains indirect, as they are not explicitly designed to address cross-frame consistency. Nevertheless, the improved frame-level accuracy lays a strong foundation for subsequent temporal refinements.

The Temporal Hungarian matching mechanism marks a substantial leap in tracking performance, as evidenced by the significant gains in temporal recall (tR@k). This innovation effectively ensures temporal coherence, reducing fragmentation in action tracklets and enabling robust tracking across video sequences. While there is a minor reduction in single-frame recall due to the fixed query assignment strategy, this trade-off is offset by the marked improvement in tracking consistency over time. The slight decline is largely attributable to query assignments occasionally defaulting to the background class, a limitation that presents an opportunity for future optimizations—such as adaptive query strategies that dynamically adjust to object motion—further harmonizing single-frame and temporal performance.

Integrating cosine similarity further strengthens temporal recall by maintaining consistency in feature representations across consecutive frames. This approach aligns with the principle that features for recurring objects or interactions should remain stable, particularly given the smooth transitions typical in video sequences. By minimizing abrupt shifts in feature vectors, the cosine similarity module enhances temporal stability, resulting in more coherent and continuous action tracklets. This synergy between components ensures that our approach excels in generating robust, temporally consistent scene graphs, particularly for challenging multi-frame scenarios.

## 7. Conclusion & Future Works

In this paper, we introduced TCDSG, an end-to-end pipeline designed to generate temporally consistent scene graphs, enabling the creation of robust action tracklets that are applicable to various downstream tasks in video-based analytics and surveillance. Our approach combines a novel modification to the bipartite matching process during training with architectural improvements, such as data-dependent initial reference points for deformable attention and a feedback loop to incorporate temporal information from previous frames. Through evaluations on three benchmark datasets, TCDSG achieved state-of-the-art results in tracklet predictions while maintaining competitive performance on single-frame predictions.

For future work, we aim to further optimize the balance between single-frame prediction accuracy and tracklet consistency, striving to enhance temporal coherence with

out sacrificing frame-level precision, especially in dynamic, multi-object environments. Additionally, leveraging the rich MEVA dataset, we plan to explore Re-identification (ReID) capabilities across distinct cameras. By focusing on cross-camera ReID, we can extend TCDSG’s capabilities to track individuals across multiple camera views, a feature highly valuable in multi-camera surveillance setups. This enhancement has the potential to enable robust tracking across complex environments, supporting continuous monitoring in large-scale applications.

## References

- [1] Yuhao Bai, Baohua Zhang, Naimin Xu, Jun Zhou, Jiayou Shi, and Zhihua Diao. Vision-based navigation and guidance for agricultural autonomous vehicles and robots: A review. *Computers and Electronics in Agriculture*, 205: 107584, 2023. [1](#)
- [2] Alex Bewley, Zongyuan Ge, Lionel Ott, Fabio Ramos, and Ben Upcroft. Simple online and realtime tracking. In *2016 IEEE international conference on image processing (ICIP)*, pages 3464–3468. IEEE, 2016. [2](#)
- [3] Nicolas Carion, Francisco Massa, Gabriel Synnaeve, Nicolas Usunier, Alexander Kirillov, and Sergey Zagoruyko. End-to-end object detection with transformers. In *European conference on computer vision*, pages 213–229. Springer, 2020. [3](#), [4](#)
- [4] Long Chen, Hanwang Zhang, Jun Xiao, Xiangnan He, Shiliang Pu, and Shih-Fu Chang. Counterfactual critic multi-agent training for scene graph generation. In *Proceedings of the IEEE/CVF International Conference on Computer Vision*, pages 4613–4623, 2019. [2](#)
- [5] Yanan Chen, Ang Li, Dan Wu, and Liang Zhou. Toward general cross-modal signal reconstruction for robotic teleoperation. *IEEE Transactions on Multimedia*, 2023. [1](#)
- [6] Bowen Cheng, Ishan Misra, Alexander G Schwing, Alexander Kirillov, and Rohit Girdhar. Masked-attention mask transformer for universal image segmentation. In *Proceedings of the IEEE/CVF conference on computer vision and pattern recognition*, pages 1290–1299, 2022. [7](#)
- [7] Meng-Jiun Chiou, Henghui Ding, Hanshu Yan, Changhu Wang, Roger Zimmermann, and Jiashi Feng. Recovering the unbiased scene graphs from the biased ones. In *Proceedings of the 29th ACM International Conference on Multimedia*, pages 1581–1590, 2021. [2](#)
- [8] Yuren Cong, Hanno Ackermann, Wentong Liao, Michael Ying Yang, and Bodo Rosenhahn. Nodis: Neural ordinary differential scene understanding. In *European Conference on Computer Vision*, pages 636–653. Springer, 2020. [2](#)
- [9] Yuren Cong, Wentong Liao, Hanno Ackermann, Bodo Rosenhahn, and Michael Ying Yang. Spatial-temporal transformer for dynamic scene graph generation. In *Proceedings of the IEEE/CVF international conference on computer vision*, pages 16372–16382, 2021. [2](#), [3](#)
- [10] Kellie Corona, Katie Osterdahl, Roderic Collins, and Anthony Hoogs. Meva: A large-scale multiview, multimodal video dataset for activity detection. In *Proceedings of the IEEE/CVF Winter Conference on Applications of Computer Vision (WACV)*, pages 1060–1068, 2021. [6](#)
- [11] Dima Damen, Hazel Doughty, Giovanni Maria Farinella, Sanja Fidler, Antonino Furnari, Evangelos Kazakos, Davide Moltisanti, Jonathan Munro, Toby Perrett, Will Price, and Michael Wray. Scaling egocentric vision: The epic-kitchens dataset. In *European Conference on Computer Vision (ECCV)*, 2018. [5](#)
- [12] Ishan Dave, Zacchaeus Scheffer, Akash Kumar, Sarah Shiraz, Yogesh Singh Rawat, and Mubarak Shah. Gabriellav2: Towards better generalization in surveillance videos for action detection. In *Proceedings of the IEEE/CVF Winter Conference on Applications of Computer Vision*, pages 122–132, 2022. [7](#)
- [13] Chen Gao, Jiarui Xu, Yuliang Zou, and Jia-Bin Huang. Drg: Dual relation graph for human-object interaction detection. In *Proc. European Conference on Computer Vision (ECCV)*, 2020. [2](#)
- [14] Kristen Grauman, Andrew Westbury, Eugene Byrne, Zachary Chavis, Antonino Furnari, Rohit Girdhar, Jackson Hamburger, Hao Jiang, Miao Liu, Xingyu Liu, et al. Ego4d: Around the world in 3,000 hours of egocentric video. In *Proceedings of the IEEE/CVF Conference on Computer Vision and Pattern Recognition*, pages 18995–19012, 2022. [5](#)
- [15] Kaiming He, Xiangyu Zhang, Shaoqing Ren, and Jian Sun. Deep residual learning for image recognition. In *Proceedings of the IEEE conference on computer vision and pattern recognition*, pages 770–778, 2016. [6](#)
- [16] Zhi Hou, Baosheng Yu, Yu Qiao, Xiaojiang Peng, and Dacheng Tao. Detecting human-object interaction via fabricated compositional learning. In *Proceedings of the IEEE/CVF Conference on Computer Vision and Pattern Recognition*, pages 14646–14655, 2021. [1](#)
- [17] Zhi Hou, Baosheng Yu, and Dacheng Tao. Discovering human-object interaction concepts via self-compositional learning. In *ECCV*, 2022. [1](#)
- [18] A S M Iftekhar, Raphael Ruschel, Satish Kumar, Suya You, and B. S. Manjunath. Dds: Decoupled dynamic scene-graph generation network. *arXiv preprint arXiv:2301.07666*, 2023. [1](#), [2](#), [3](#), [7](#)
- [19] Loshchilov Ilya, Hutter Frank, et al. Decoupled weight decay regularization. *Proceedings of ICLR*, 2019. [6](#)
- [20] Jingwei Ji, Ranjay Krishna, Li Fei-Fei, and Juan Carlos Niebles. Action genome: Actions as compositions of spatio-temporal scene graphs. In *Proceedings of the IEEE/CVF Conference on Computer Vision and Pattern Recognition*, pages 10236–10247, 2020. [5](#)
- [21] Jingwei Ji, Rishi Desai, and Juan Carlos Niebles. Detecting human-object relationships in videos. In *Proceedings of the IEEE/CVF International Conference on Computer Vision*, pages 8106–8116, 2021. [2](#)
- [22] Justin Johnson, Ranjay Krishna, Michael Stark, Li-Jia Li, David Shamma, Michael Bernstein, and Li Fei-Fei. Image retrieval using scene graphs. In *Proceedings of the IEEE conference on computer vision and pattern recognition*, pages 3668–3678, 2015. [2](#)

[23] Siddhesh Khandelwal and Leonid Sigal. Iterative scene graph generation. *Advances in Neural Information Processing Systems*, 35:24295–24308, 2022. 7

[24] Laura Leal-Taixé, Cristian Canton-Ferrer, and Konrad Schindler. Learning by tracking: Siamese cnn for robust target association. In *Proceedings of the IEEE conference on computer vision and pattern recognition workshops*, pages 33–40, 2016. 2

[25] Xiangtai Li, Wenwei Zhang, Jiangmiao Pang, Kai Chen, Guangliang Cheng, Yunhai Tong, and Chen Change Loy. Video k-net: A simple, strong, and unified baseline for video segmentation. In *Proceedings of the IEEE/CVF Conference on Computer Vision and Pattern Recognition*, pages 18847–18857, 2022. 1, 7

[26] Yiming Li, Xiaoshan Yang, and Changsheng Xu. Dynamic scene graph generation via anticipatory pre-training. In *Proceedings of the IEEE/CVF Conference on Computer Vision and Pattern Recognition*, pages 13874–13883, 2022. 7

[27] Yong-Lu Li, Siyuan Zhou, Xijie Huang, Liang Xu, Ze Ma, Hao-Shu Fang, Yanfeng Wang, and Cewu Lu. Transferable interactiveness knowledge for human-object interaction detection. In *Proceedings of the IEEE Conference on Computer Vision and Pattern Recognition*, pages 3585–3594, 2019. 2

[28] Tsung-Yi Lin, Michael Maire, Serge Belongie, James Hays, Pietro Perona, Deva Ramanan, Piotr Dollár, and C Lawrence Zitnick. Microsoft coco: Common objects in context. In *European conference on computer vision*, pages 740–755. Springer, 2014. 6

[29] Xin Lin, Chong Shi, Yibing Zhan, Zuopeng Yang, Yaqi Wu, and Dacheng Tao. Td2-net: Toward denoising and debiasing for dynamic scene graph generation. *ArXiv*, abs/2401.12479, 2024. 2, 7

[30] Xiaochen Liu, Pradipta Ghosh, Oytun Ulutan, B. S. Manjunath, Kevin Chan, and Ramesh Govindan. Caesar: cross-camera complex activity recognition. In *Proceedings of the 17th Conference on Embedded Networked Sensor Systems*, page 232–244, New York, NY, USA, 2019. Association for Computing Machinery. 1

[31] Yang Liu, Qingchao Chen, and Andrew Zisserman. Amplifying key cues for human-object-interaction detection. In *European Conference on Computer Vision*, pages 248–265. Springer, 2020. 2

[32] Jiale Lu, Lianggangxu Chen, Youqi Song, Shaohui Lin, Changbo Wang, and Gaoqi He. Prior knowledge-driven dynamic scene graph generation with causal inference. In *Proceedings of the 31st ACM International Conference on Multimedia*, page 4877–4885, New York, NY, USA, 2023. Association for Computing Machinery. 2, 7

[33] Yichao Lu, Himanshu Rai, Jason Chang, Boris Knyazev, Guangwei Yu, Shashank Shekhar, Graham W Taylor, and Maksims Volkovs. Context-aware scene graph generation with seq2seq transformers. In *Proceedings of the IEEE/CVF International Conference on Computer Vision*, pages 15931–15941, 2021. 2

[34] Tim Meinhardt, Alexander Kirillov, Laura Leal-Taixé, and Christoph Feichtenhofer. Trackformer: Multi-object tracking with transformers. In *Proceedings of the IEEE/CVF conference on computer vision and pattern recognition*, pages 8844–8854, 2022. 3

[35] Sayak Nag, Kyle Min, Subarna Tripathi, and Amit K. Roy-Chowdhury. Unbiased scene graph generation in videos. In *2023 IEEE/CVF Conference on Computer Vision and Pattern Recognition (CVPR)*, pages 22803–22813, 2023. 1, 2, 7

[36] Jing Qi, Li Ma, Zhenchao Cui, and Yushu Yu. Computer vision-based hand gesture recognition for human-robot interaction: a review. *Complex & Intelligent Systems*, 10(1):1581–1606, 2024. 1

[37] Raphael Ruschel, A. S. M. Iftekhar, B. S. Manjunath, and Suya You. Bload: Enhancing neural network training with efficient sequential data handling. *arXiv preprint arXiv:2310.10879*, 2023. 6

[38] Samuel Schulter, Paul Vernaza, Wongun Choi, and Manmohan Chandraker. Deep network flow for multi-object tracking. In *Proceedings of the IEEE Conference on Computer Vision and Pattern Recognition*, pages 6951–6960, 2017. 2

[39] Xindi Shang, Donglin Di, Junbin Xiao, Yu Cao, Xun Yang, and Tat-Seng Chua. Annotating objects and relations in user-generated videos. In *Proceedings of the 2019 on International Conference on Multimedia Retrieval*, pages 279–287. ACM, 2019. 5

[40] Jing Shi, Yiwu Zhong, Ning Xu, Yin Li, and Chenliang Xu. A simple baseline for weakly-supervised scene graph generation. In *Proceedings of the IEEE/CVF International Conference on Computer Vision*, pages 16393–16402, 2021. 2

[41] Gunnar A Sigurdsson, Gülden Varol, Xiaolong Wang, Ali Farhadi, Ivan Laptev, and Abhinav Gupta. Hollywood in homes: Crowdsourcing data collection for activity understanding. In *European Conference on Computer Vision*, pages 510–526. Springer, 2016. 5

[42] Peize Sun, Jinkun Cao, Yi Jiang, Rufeng Zhang, Enze Xie, Zehuan Yuan, Changhu Wang, and Ping Luo. Trantrack: Multiple object tracking with transformer. *arXiv preprint arXiv:2012.15460*, 2020. 3

[43] Kaihua Tang, Hanwang Zhang, Baoyuan Wu, Wenhan Luo, and Wei Liu. Learning to compose dynamic tree structures for visual contexts. In *Proceedings of the IEEE/CVF conference on computer vision and pattern recognition*, pages 6619–6628, 2019. 2

[44] Yao Teng, Limin Wang, Zhifeng Li, and Gangshan Wu. Target adaptive context aggregation for video scene graph generation. In *Proceedings of the IEEE/CVF International Conference on Computer Vision*, pages 13688–13697, 2021. 2

[45] Oytun Ulutan, ASM Iftekhar, and Bangalore S Manjunath. Vsgnet: Spatial attention network for detecting human object interactions using graph convolutions. In *Proceedings of the IEEE/CVF Conference on Computer Vision and Pattern Recognition*, pages 13617–13626, 2020. 2

[46] Bo Wan, Desen Zhou, Yongfei Liu, Rongjie Li, and Xuming He. Pose-aware multi-level feature network for human object interaction detection. In *Proceedings of the IEEE International Conference on Computer Vision*, pages 9469–9478, 2019. 2

[47] Guan Wang, Zhimin Li, Qingchao Chen, and Yang Liu. Oed: Towards one-stage end-to-end dynamic scene graph generation. In *Proceedings of the IEEE/CVF Conference on Computer Vision and Pattern Recognition*, pages 27938–27947, 2024. 7

[48] Suchen Wang, Yueqi Duan, Henghui Ding, Yap-Peng Tan, Kim-Hui Yap, and Junsong Yuan. Learning transferable human-object interaction detector with natural language supervision. In *Proceedings of the IEEE/CVF Conference on Computer Vision and Pattern Recognition*, pages 939–948, 2022. 1

[49] Shuang Wang, Lianli Gao, Xinyu Lyu, Yuyu Guo, Pengpeng Zeng, and Jingkuan Song. Dynamic scene graph generation via temporal prior inference. In *Proceedings of the 30th ACM International Conference on Multimedia*, page 5793–5801, New York, NY, USA, 2022. Association for Computing Machinery. 3, 7

[50] Tiancai Wang, Rao Muhammad Anwer, Muhammad Haris Khan, Fahad Shahbaz Khan, Yanwei Pang, Ling Shao, and Jorma Laaksonen. Deep contextual attention for human-object interaction detection. In *Proceedings of the IEEE International Conference on Computer Vision*, pages 5694–5702, 2019. 2

[51] Wenbin Wang, Ruiping Wang, Shiguang Shan, and Xilin Chen. Exploring context and visual pattern of relationship for scene graph generation. In *Proceedings of the IEEE/CVF Conference on Computer Vision and Pattern Recognition*, pages 8188–8197, 2019. 2

[52] Wenbin Wang, Ruiping Wang, and Xilin Chen. Topic scene graph generation by attention distillation from caption. In *Proceedings of the IEEE/CVF International Conference on Computer Vision*, pages 15900–15910, 2021. 2

[53] Zhongdao Wang, Hengshuang Zhao, Ya-Li Li, Shengjin Wang, Philip Torr, and Luca Bertinetto. Do different tracking tasks require different appearance models? *Advances in Neural Information Processing Systems*, 34:726–738, 2021. 7

[54] G Welch. An introduction to the kalman filter. 1995. 2

[55] Nicolai Wojke, Alex Bewley, and Dietrich Paulus. Simple online and realtime tracking with a deep association metric. In *2017 IEEE international conference on image processing (ICIP)*, pages 3645–3649. IEEE, 2017. 2

[56] Jingkang Yang, Wenzuan Peng, Xiangtai Li, Zujin Guo, Liangyu Chen, Bo Li, Zheng Ma, Kaiyang Zhou, Wayne Zhang, Chen Change Loy, and Ziwei Liu. Panoptic video scene graph generation. In *CVPR*, 2023. 1, 2, 5, 7

[57] Fangao Zeng, Bin Dong, Yuang Zhang, Tiancai Wang, Xiangyu Zhang, and Yichen Wei. Motr: End-to-end multiple-object tracking with transformer. In *European Conference on Computer Vision*, pages 659–675. Springer, 2022. 3

[58] Ji Zhang, Kevin J Shih, Ahmed Elgammal, Andrew Tao, and Bryan Catanzaro. Graphical contrastive losses for scene graph parsing. In *Proceedings of the IEEE/CVF Conference on Computer Vision and Pattern Recognition*, pages 11535–11543, 2019. 2

[59] Huiyu Zhou, Yuan Yuan, and Chunmei Shi. Object tracking using sift features and mean shift. *Computer vision and image understanding*, 113(3):345–352, 2009. 2

[60] Xizhou Zhu, Weijie Su, Lewei Lu, Bin Li, Xiaogang Wang, and Jifeng Dai. Deformable detr: Deformable transformers for end-to-end object detection. *arXiv preprint arXiv:2010.04159*, 2020. 3, 4